Response of human bone marrow stromal cells to a resorbable P2O5–SiO2–CaO–MgO–Na2O–K2O phosphate glass ceramic for tissue engineering applications

Response of human bone marrow stromal cells to a novel phosphate glass-ceramic for tissue engineering applications

E. Leonardi[a], G. Ciapetti[a], N. Baldini[a], G. Novajra[b], E. Verné[b], F. Baino[b], C. Vitale-Brovarone[b,*]

[a]*Laboratorio di Fisiopatologia degli Impianti Ortopedici, Istituto Ortopedico Rizzoli, Via di Barbiano 1/10, 40136 Bologna, Italy*

[b]*Materials Science and Chemical Engineering Department, Politecnico di Torino, Corso Duca degli Abruzzi 24, 10129 Torino, Italy*

*Corresponding author: chiara.vitale@polito.it

Tel.: +39 011 564 4716

Fax: +39 011 564 4699

Keywords: Phosphate glass; Glass-ceramic; Bone marrow cells; Bioactive surface; Tissue engineering.

1. Introduction

Tissue engineering aims to restore damaged tissues and/or functions in the human body by stimulating the physiological mechanism of regeneration and repair. Bioactive glasses (BGs) and glass-ceramics (BGCs) have a high potential in the field of regenerative medicine as regards both hard-tissue engineering and, more recently, soft-tissue engineering. In the early 1970s, the concept of bioactivity was defined as the ability of certain materials to bond to bone and to stimulate osteogenesis [1]; since then, BGs began to be proposed and investigated for bone implants applications. The first generation of BGs involved silicate-based glasses, in which silicon dioxide (SiO_2) acts as a network former, and other oxides, such as Na_2O, and CaO, were added to the composition as network modifiers. Bioglass®, belonging to the SiO_2–Na_2O–CaO–P_2O_5 system, was the first glass able to form an interfacial bond with living bone after implantation [2]. Since then, more complex compositions were designed to enhance the bioactivity of the material.

In the last decade, one of the major challenges of tissue engineering has been the synthesis of materials able to safely dissolve once they have performed their function, leaving the body to remodel the tissue to its natural form. To this aim a novel group of glasses involving P_2O_5 as network former have been proposed; the asymmetry of the [PO_4] tetrahedron unit, that represents the phosphate-based glass structural unit, is believed to be the origin of their low durability, together with the ease of hydration of the P–O–P bonds [3]. Phosphate glasses (PGs) have a great potential because their solubility is strongly dependent on their composition; their degradation rate can be tailored by adding metal oxides, such as TiO_2 [4-5], CuO [6] and Fe_2O_3 [7-8] to the glass composition. PGs dissolves congruently throughout the whole process [9]. The two interdependent steps that take place during glass dissolution are the hydration reaction, with a Na–H ion exchange, and the network breakage in the hydrated layer due to the destruction of the P–O–P bonds [3]. PGs have been widely studied as a controlled release vehicle of antibacterial ions, such as silver, copper,

zinc, gallium [10] and have been also studied for application in the field of bone tissue regeneration in the form of powder or porous scaffold, alone or with polymers in composite materials [4,11]. Nerve guide of PGs, like tubes or mesh of non-woven fibres, were developed and tested in vivo [12-13] with good results and 3-D constructs for the repair of the muscular tissue have been also studied [14].

In this work, a novel phosphate-based glass-ceramic (GC-ICEL) was synthesised and characterized in terms of crystalline structure, solubility and biological compatibility. It is known that the events occurring at the glass surface, *i.e.* adsorption of molecules and growth factors, lead to integrin activation and cell adhesion [15]. As described for other glass substrates [16], the immersion of GC-ICEL in α-minimum essential medium (α-MEM) may trigger a continuous ion-exchange between the surface and the solution. The aim of the cell-based studies presented in this work was to evaluate the effect of GC-ICEL on adhesion, proliferation and gene expression of osteoblastic markers of human marrow-derived stromal cells (hMSCs).

2. Materials and Methods

2.1. Synthesis of glass

The starting phosphate-based glass belonged to the P_2O_5–SiO_2–CaO–MgO–Na_2O–K_2O system (ICEL) [17], and had the following molar composition: 45% P_2O_5, 3% SiO_2, 26% CaO, 7% MgO, 15% Na_2O, 4% K_2O. ICEL was prepared by melting the raw products, *i.e.* $(NH_4)_2HPO_4$, SiO_2, $Ca_3(PO_4)_2$, $Mg_3(PO_4)_2 \cdot 8H_2O$, $Na_3PO_4 \cdot 12H_2O$ and K_2HPO_4, in a platinum crucible at 1,200 °C in air for 1 h to ensure homogeneity (heating rate set at 10 °C·min^{-1}). The molten glass was cast into moulds to produce bars that were cut by a diamond rotating wheel (Struers Accutom 5). The glass pieces were ground by ball milling to obtain powders which were sieved below 30 μm.

2.2. Preparation of glass-ceramic samples

Massive glass-ceramic ICEL (GC-ICEL) samples were obtained via uniaxial dry pressing of as-poured glass powders sieved below 30 μm and by a suitable thermal treatment. Both disk-shaped and bar-shaped "green" compacts were produced depending on the end use. Specifically, the disks were used for GC-ICEL morphological, structural and *in vitro* characterization, whereas the bars were cut into slices for the biological assessment. Both samples (disks and slices) were produced with surface area of ~50 mm^2 and thickness of ~2 mm. The applied pressure and time were set in order to obtain crack-free "greens"; the optimal conditions were identified with 135 MPa/10 s for the bars and with 90 MPa/60 s for the disks. The "green" bodies were thermally treated at 610 °C for 3 h to sinter ICEL powders (heating and cooling rate were set at 5 and 10 $°C \cdot min^{-1}$, respectively). The sintering conditions were set on the basis of hot stage microscopy and thermal analysis data, reported elsewhere [17], to achieve an effective densification of the samples.

2.3. Evaluation of GC-ICEL solubility

Solubility tests were performed on GC-ICEL disks to evaluate the erosion rate and the dissolution kinetics of the material. The study was developed according to the ISO standard [18], by soaking the samples for different time frames in 25 ml of three media mimicking, with various approximation degrees, the biological fluids: distilled water, Tris-HCl and acellular simulated body fluid (SBF) [19]. Specifically, GC-ICEL samples were maintained at 37 °C in polyethylene bottles; a refresh of the solutions occurred every 48 h to approximately simulate fluid circulation in the human body.

GC-ICEL solubility was assessed by calculating the weight loss of the samples after 7 days and 1, 2, 3 months of soaking in the three different media. After soaking the samples were extracted from

the solutions, dried at room temperature for 24 h and finally weighted. The per cent weight loss Λ_W (%) was assessed as

$$\Lambda_W = \left(\frac{W_0 - W_s}{W_0} \right) \times 100,$$

where W_0 and W_s are, respectively, the scaffold weight before and after soaking.

As the solubility is affected by the surface area, the weight loss per unit area Λ_S (mg·cm^{-2}) was assessed as

$$\Lambda_S = \frac{W_0 - W_s}{S},$$

where S (cm^2) is the external surface exposed to the solution.

The tests were performed on triplicate samples for every time frame; the reported values of weight loss are an average of the acquired data. During soaking, the variations of pH in the solutions, due to ion-leaching phenomena, were daily monitored. GC-ICEL samples were investigated before and after soaking in distilled water, Tris-HCl and SBF by means of wide-angle (2θ within 10-70°) X-ray diffraction (XRD; X'Pert Philips diffractometer with Bragg Brentano camera geometry and Cu Kα incident radiation). In addition, the samples underwent scanning electron microscopy (SEM) and compositional analysis by using a Philips 525M SEM apparatus equipped with Edax Philips 9100 for energy dispersive spectroscopy (EDS), to evaluate the modifications occurring on their surface owing to erosion phenomena.

2.4. Biological tests

2.4.1. Sample preparation

The samples were weighed, in dry conditions, prior to cell seeding and after cell removal at each time points, to verify any weight loss during *in vitro* testing. Sterilization was obtained by soaking the samples first in 70% ethanol (2 h) and then in 1% antibiotic/antimycotic in phosphate-buffered

saline (PBS) (2 h). Finally, a pre-wetting step in 10% serum-added medium (1.5 h) was performed to improve cells adhesion.

2.4.2. Cell isolation

hMSCs were isolated from bone marrow tissue during total hip replacement surgery. Written consent from patients was obtained, and the tissue collection was approved by the Institutional Ethical Committee. Heparinized femoral-shaft marrow was layered onto Ficoll gradient and mononuclear cells (MNCs) were collected at the interface after centrifugation at 4000×*g* for 0.5 h. MNCs were plated in polystyrene flasks and incubated with α-MEM, 10% foetal bovine serum, 2 mM glutamine and 1% antibiotic (penicillin/streptomycin) solution (standard medium) at 37°C in 5% CO_2, and non-adherent cells were removed after 4 days. Adherent hMSCs were sub-cultured with standard medium added with 50 $\mu g \cdot ml^{-1}$ ascorbate-2 phosphate and splitted at sub-confluence. Second passage cells were used for GC-ICEL experiments.

2.4.3. Cell seeding and culture

Cells were seeded at a density of $2.5 \cdot 10^4$ $cells \cdot cm^{-2}$ by applying 25 µl of cell suspension to the samples and incubated at 37 °C for 1 h in wet chamber to allow for cell attachment; then 1 ml of medium was added to fill the well. hMSCs, seeded in tissue culture plastic (TCPS) at $2.5 \cdot 10^4$ $cell \cdot cm^{-2}$ in 24-well plates, provided the controls. Cell seeding efficiency, that is the number of attached cells expressed as percent of the cells seeded, was calculated 24 h after plating using Picogreen assay; the mean DNA content of our cells was defined by interpolation of the values on a reference curve. Then the number of cells was calculated from the Picogreen test results. Cells were fed twice a week with osteogenic medium, *i.e.* standard medium plus 10^{-8} M dexamethasone and 10 mM β-glycerophosphate. At 1, 7 and 14 days, morphological, biochemical and molecular assays were performed.

2.4.4. Morphological assays

Cell morphology of hMSCs on TCPS was monitored by light microscopy throughout the culture period. In order to investigate cell morphology and spreading on samples, hMSC were stained with two different dyes and observed by fluorescence microscopy (Nikon). Cytoskeleton was visualized following staining of actin filaments with rhodamine-phalloidin fluorochrome. Cells fixed with 2% paraformaldehyde were permeabilized with 0.5% Triton X-100. Then, the cells were incubated for 45 minutes at room temperature in the dark with rhodamine-phalloidin 1:200 in PBS (0.06 μM, Molecular Probes, Eugene, OR). For acridine orange staining, following fixation in 3.7% paraformaldehyde and permeabilization with 0.1% Triton-X100, the cells were incubated with 6 $\mu g \cdot ml^{-1}$ acridine orange in EDTA-buffer. Ultrastructural analysis was carried out by SEM after the cell-seeded samples were treated as already described [20].

2.4.5. Biochemical assays

The pH of supernatant covering the cell-seeded slices was measured 3 times a week by using colorimetric stripes (range 6.0-8.0, Merck). Alamar Blue test (Biosource International-CA) was used to asses cell viability. Briefly, Alamar Blue solution was added (10%vol.) to the culture wells. After incubation for 4 h at 37 °C the medium was transferred in another plate and the fluorescence measured using a CytoFluor 2350 plate reader (Millipore Corporation, Bedford, MA, USA) with 490/530 nm of excitation/emission wavelength. Results were expressed as RFUs (Relative Fluorescence Units) normalized to the number of cells seeded.

DNA content was quantified by Picogreen assay (Quant-IT Picogreen dsDNA, Invitrogen): cells were lysed with 0.01% SDS and sonication, and 10 μl of cell lysate or standard were mixed with 10 μl of Picogreen solution in wells of a 96-well plate. The fluorescence was read at 480-520 nm with Cytofluor.

Alkaline phosphatase (ALP) activity was measured by a chromogenic assay based on conversion of p-nitrophenyl phosphate substrate to p-nitrophenol. ALP reaction buffer was added 1:1 to cell

lysates and the mixture incubated at 37 °C for 15 minutes. The absorption was measured at 405 nm with a spectrophotometer for microplates (Spectra III, Tecan, Austria), and phosphatase activity calculated using a calibration curve by serial dilution of p-nitrophenol standard solution. ALP activity was normalized to the DNA content, used as an index of the cell number.

Synthesis of type I collagen was assessed by measuring its metabolic product released in the supernatant. Levels of C-terminal propeptide of type I collagen (CICP) were quantified by enzyme immunoassay according to the manufacturer's instructions (Quidel corporation, Heidelberg, Germany).

2.4.6. Molecular assay: gene expression analysis

The gene expression analysis was performed at 24 h (only on control cells), 7 days and 14 days, by quantifying the transcripts of genes useful to monitor the hMSCs differentiation to osteoblasts, as reported in Table 1. RNA was extracted with an RNeasy mini kit (Qiagen, GmbH, Hilden, Germany) and the retrotranscription was performed with MuLV Reverse Transcriptase (Applied Biosystems, Foster City, CA, USA). For real time polymerase chain reaction 1.5 μg of cDNA were amplified with the Light Cycler instrument and the Universal Probe Library system (Roche Applied Science, Monza, Italy) [21]. Probes and primers were selected using a web-based assay design software [ProbeFinder, https://www.roche-applied-science.com]. The results were expressed as a ratio between gene of interest and GAPDH reference gene.

2.4.7. Statistics

Results are reported as mean ± standard error of three separate experiments on duplicate samples and controls.. Differences in gene expression, DNA, and ALP content were assessed using analysis of variance (Kruskal-Wallis test); Mann–Whitney test was performed as a *post hoc* test of the multiple analyses, or as unpaired comparison for 2 independent variables. The level of statistical significance was established at $p < 0.05$.

3. Results

3.1. GC-ICEL

As-poured ICEL is a completely amorphous glass, as assessed in a previous work [17]. XRD spectra of GC-ICEL before and after soaking in water, SBF and Tris-HCl were compared in figure 1. The thermal treatment of sintering led to the nucleation of two crystalline phases whose main peaks were marked in the XRD pattern. Specifically, the two phases were identified as $Na_2Mg(PO_4)_3$ (sodium/magnesium phosphate, PDF reference code 00-022-0477) and $Ca_2P_2O_7$ (calcium pyrophosphate, PDF reference code 00-033-0297).

After soaking for 7 days in the three different media, a partial dissolution of $Na_2Mg(PO_4)_3$ crystals occurs, as confirmed by the disappearance of the peaks at $2\theta = 17.9°$ and at $2\theta = 19.2°$ identifying this phase. Moreover, the intensity of the other peaks associated to this phase progressively decreases as the soaking time increases. After 3 months of soaking in water and Tris-HCl, this phenomenon is clearly evident. Concerning the samples soaked for 3 months in SBF, a different behaviour was observed. The peaks corresponding to GC-ICEL crystalline phases are masked by a newly formed phase, which exhibits a main broad peak at $2\theta \approx 32°$ and was identified as apatite-like.

SEM analysis was performed on GC-ICEL before and after soaking in water and in SBF, in order to evaluate the modifications occurring in the samples. Figure 2a shows as-done GC-ICEL surface at low magnification. A diffuse microporosity, due to the sintering process, can be seen. In figure 2b the glass-ceramic nature of the sample is clearly visible, as assessed by XRD data previously reported (figure 1). Compositional analysis assessed that the needle-shaped crystals, particularly evident in figure 2b, belong to calcium pyrophosphate ($Ca_2P_2O_7$).

The surface of GC-ICEL soaked for 7 days in distilled water is depicted in figure 3: a lot of pits can be seen due to the high surface erosion rate in water and to the dissolution of the residual

amorphous phase. Similar surface modifications and erosions was found on the samples soaked in Tris-HCl. GC-ICEL surface after 3 months in SBF is shown in figure 4; globe-shaped agglomerates of a newly formed phase are clearly distinguishable. EDS compositional analysis (not reported) revealed that this phase is constituted by Ca and P, thus demonstrating the formation of an apatite-like layer on GC-ICEL surface and confirming the results of XRD investigations (figure 1b). In addition, the newly formed phase exhibits a "cauliflower" morphology very similar to that of hydroxyapatite (HA) formed on bioactive glasses.

The weight losses calculated by solubility tests are reported in table 2. A more immediate evaluation of weight loss trend is reported as bars chart in figure 5. As expected, the erosion rate in the three media increases over the time, due to the progressive release of phosphates in the solutions. The highest dissolution is obtained in water, where the weight loss is almost 50% after 3 months. GC-ICEL shows a weight loss of about 30% in Tris-HCl and of about 10% in SBF after 3 months. For the GC-ICEL soaked in SBF there is an evident decrease in the weight loss rate after the first month. The pH changes are remarkable for the dissolution test in water (variation between 5.20 and 7.60) and are more moderate in Tris-HCl (variation between 7.30 and 7.50) and in SBF (variation between 7.35-7.45).

3.2. Biological tests

3.2.1. GC-ICEL/medium interactions

The pH of the culture medium was measured to check if ions released by GC-ICEL affect the optimal culture condition. It has been found that the pH was not significantly altered in hMSC-seeded samples: the values, ranging between 6.8 and 7.1 during the 2 weeks-culture period, were well tolerated by the cells (figure 6). Regarding sample degradation in the culture medium, after 2

weeks of culture GC-ICEL slices had lost 5.2 % of their initial weight, with most of this loss occurring in the first 24 h after cell seeding.

3.2.2. Cell adhesion at early time point

The seeding efficiency on GC-ICEL slices was 33.8% ± 6.2%. At the early time-point hMSCs were observed to attach on the material surface, even if they are not yet completely elongated and spindle-shaped, and actin cytoskeleton, highlighted by TRITC-labelled phalloidin staining, is not yet organized (figure 7a,b). Cells on TCPS spread with elongated stress fibers (figure 7c,d). Ultrastructural analysis by SEM showed anchoring processes extended from cells and confirmed that, at 1 day from seeding, hMSCs are able to attach to the surface, as well as surround macropores and establish intercellular contacts (figure 8a,b).

3.2.3. Cell viability and proliferation

The viability of hMSCs grown on GC-ICEL slices was good. GC-ICEL did not altered the proliferation rate of hMSCs, that increased their metabolic activity progressively along the whole culture time period (figure 9a). The DNA content of control cells became higher along the culture, as well. On the contrary, DNA of hMSCs on samples raised during the first 7 days and then stopped to augment and, at 14 days, returned to the initial value (figure 9b).

The values of quantitative parameters for cell number were found to be significantly higher on TCPS compared to the same time point on GC-ICEL surfaces, as expected from seeding efficiency results.

The ultrastructural details of GC-ICEL were observed with or without cells (figure 10), and, as it can be observed, the pre-wetting treatment with serum did not alter the material surface, apart from the already assessed bioerosion process dissolving preferentially the residual amorphous phase and the $Na_2Mg(PO_4)_3$ crystals. At 7 days the cells are more elongated compared to the 1-day view, grow in clusters, and cytoplasmic prolongations are firmly attached to glass-ceramic asperities (figure

10c-d). At 14 days of culture on GC-ICEL samples the hMSCs were not confluent, and their number was just slightly increased compared to 7 days: this confirms the biochemical data indicating that cells are quiescent between the 1st and 2nd week of culture (figure 10e,f).

3.2.4. Osteogenic differentiation

The alkaline phosphatase activity, marker of early osteogenic differentiation, decreased over time; while on TCPS the more significant decrease occurred between 1 and 7 days, in hMSCs grown on GC-ICEL, ALP was stable in the 1st week and diminished dramatically from 7 to 14 days (figure 11a). hMSCs cultured on GC-ICEL were able to produce type I collagen and the amount increased progressively along the culture period (figure 11b). Cells grown on TCPS as controls showed a similar behaviour over time, with a statistical significant increase from 24 h to 7 days.

Concerning gene expression, the RNA yield was lower than expected, possibly due to GC-ICEL ion release interfering with the procedure of RNA extraction (based on ion exchange). As a consequence, due to the low amount of transcripts, some results were close to the detection limit of the assay, and not always included in the analysis (figure 12). Expression of ALP transcript mirrored the protein activity and slightly decreased in samples and controls, even if the differences were not statistically significant, owing to the quite large standard errors of the means. Collagen type I gene expression showed a similar behaviour and the descendant trend was observed along the culture time. Finally, osteocalcin, late marker of osteodifferentiation, increased steadily from 1 to 14 days from seeding. Differently from the other assays, the absolute values of transcripts in cells grown on GC-ICEL were similar or higher than TCPS controls.

4. Discussion

ICEL is a phosphate-based glass developed by modifying the chemical composition of a silicate-based glass (CEL2) previously proposed and investigated [22] by the authors. The molar amounts

of SiO_2 and P_2O_5 in the ICEL composition are inverted in comparison with those of CEL2, aiming to prepare a phosphate-based glass with small amounts of silica, without any variation both of the modifier oxides amounts and of the former/modifier oxides ratio, in respect to a well investigated composition.

The presence of SiO_2 in ICEL composition was thought to increase the glass degradation rate: in fact, as reported by other authors [23], low amount of SiO_2 locally disrupts the P_2O_5-based network of the glass. In addition, it was demonstrated that silicon ions stimulate gene expression of osteoblasts in order to accelerate bone mineralization [24-26]: this can promote the *in vivo* formation of a stable interface between the glass and the surrounding living bone.

As shown in figure 1a, the sintering treatment induced the nucleation of two crystalline phases; in particular, calcium pyrophosphate ($Ca_2P_2O_7$) is known to be highly biocompatible and bioactive because, as previously reported by other authors [27,28], it can act as precursor of HA or apatite-like phases mimicking bone mineral. The role of ($Ca_2P_2O_7$) showed to be effective in imparting bioactive properties to GC-ICEL by promoting the precipitation of a thick HA layer on the GC-ICEL after soaking in SBF (figure 4). The assessed GC-ICEL bioactivity was in good accord with that reported by Monem et al. [29], who observed in vivo bone growth between phosphate glass-ceramic particles implanted into rabbit femur due to the presence of β-$Ca_2P_2O_7$ as the main phase. Furthermore, Sun et al. [30] showed that the ionic product derived by the calcium pyrophosphate dissolution is able to activate genes of the bone cells and thus the presence of a pyrophosphate phase in GC-ICEL could be of particular interest for its application in bone tissue engineering.

As regards the solubility of GC-ICEL, reported as bar charts in figure 5, some conlcusions can be drawn. The weight losses of the samples soaked in SBF are lower than those of the samples soaked in water and Tris-HCl, because the formation of a HA layer greatly balances the weight loss due to erosion. Hence, it should be noticed that the weight losses in SBF are remarkably underestimated. The presence of newly formed HA agglomerates was expected to affect the GC-ICEL dissolution in SBF: specifically, the hydrolysis of the phosphate chains was hampered as the precipitated HA

layer can act as a diffusion barrier of water molecules, that will reach the GC-ICEL surface in lower amounts and at lower rate. The precipitation of a thick HA layer and its barrier diffusion effect can explain the drastic decrease in the weight loss rate of GC-ICEL after the first month of soaking in SBF. However, the overall rate of dissolution is higher than that of HA precipitation, leading to a net weight loss. The GC-ICEL solubility in Tris-HCl is higher than that in SBF, but definitely lower than that in distilled water, in which the maximum dissolution rate was observed. These results are consistent with XRD and SEM investigations: in fact, both in Tris-HCl and in water no precipitation of HA occurred and, therefore, the weight loss was not counterbalanced.

The pH lowering in distilled water is caused by the release of the acid dissolution product of GC-ICEL, although the medium was refreshed every 48 h. In SBF and Tris-HCl, which are buffer solutions, this phenomenon is almost avoided. Since the dissolution process of phosphate glasses is very sensitive to pH [3], the solubility is higher in distilled water than in Tris-HCl and SBF.

As GC-ICEL is a glass-ceramic material, apart from the congruent dissolution of the residual amorphous phase, the two crystalline phases showed a very different behaviour. In fact XRD results (reported in figure 1) showed the dissolution of the sodium/magnesium phosphate ($Na_2Mg(PO_4)_3$) phase, while any significant difference was observed in the diffraction peaks of the calcium pyrophosphate ($Ca_2P_2O_7$). This is due to the low solubility of this phase, as reported by other authors [27].

The tests carried out to assess the biological compatibility of GC-ICEL demonstrated that the material is not toxic for human marrow-derived cells, which showed a time-dependent proliferation on its surface over a 14-days period. Collagen and ALP production confirm that hMSCs cultured with the osteogenic inducers on GC-ICEL substrates go toward bone differentiation. The apparent contrast between the results of the viability test and the DNA content may be due to the formation on the GC-ICEL surface of an extracellular matrix which restricts cell proliferation to stimulate differentiation. This hypothesis, which is also suggested by other authors in a study on bioactive glass particles and osteoblasts [31], is supported by the decrease of ALP between 7 and 14 days,

whereas collagen steadily increase in the same period, to provide the main structural component of extracellular matrix (ECM). In such a condition, the cells remain metabolically active, thus converting Alamar blue to formazan deposits, but most of the quiescent cells are entrapped within the matrix and can not be easily removed from the surface. As a consequence of these effects, DNA measured in the cell lysate is reduced at the final endpoint. It has to be noticed that Augst *et al.* found a similar time-course of DNA production between 3 and 6 weeks in human mesenchymal stem cells cultured under continuous osteogenic induction in the bone region of an osteochondral composite, despite the condition of dynamic culture obtained with a bioreactor [32]. The decrease of ALP activity during culture on a bioactive glass has been observed by Jones *et al.* [33], who found a peak of ALP released by osteoblasts on a phosphate-free bioactive glass at 14 days, to be followed by a decrease at 21 days. A production of collagen type I by GC-ICEL seeded cells higher than that recorded by TCPS-seeded cells was found, too, by the same Authors. At RNA level, ALP transcript decreased, in agreement with ALP enzyme activity, while collagen type I gene expression diminished whereas protein expression was enhanced. This can be due to different half-life of the targeted protein compared with the respective mRNA: the protein might still be present, while the RNA has already been degraded [34]. The gene expression pattern of ALP, collagen I and osteocalcin, markers of osteogenic differentiation, suggested that hMSCs grown on GC-ICEL reached a late differentiation in the 14 days culture, as cells on TCPS did, confirming that they retain their bone-forming potential [35].

In summary, concerning the interaction of GC-ICEL and cells, following initial adhesion and some proliferation the human marrow stromal cells did not reach confluency on the glass surface. Different mechanisms for this behavior may be suggested, including rapid changes of the surface chemistry, as described in the soaking assays, which may hamper cell proliferation, or partial degradation of the outer layer due to frequent changes of the medium, or an unfavourable topography of the glass surface. The formation of an apatite-like layer, which could have been osteconductive, was shown after 3 months in SBF; hence, during *in vitro* culture the cells were

likely to grow on a different substrate. Nonetheless, under osteogenic stimulus, the human marrow stromal cells on GC-ICEL differentiated to osteoblast lineage, as shown by ALP and collagen type I production, as well as gene expression for ALP, collagen I and osteocalcin.

5. Conclusions

GC-ICEL showed to be bioactive when soaked in a simulated body fluid as the precipitation of a continuous layer of HA was observed; this is probably due to the bioactive role of $Ca_2P_2O_7$ crystals. GC-ICEL is a resorbable glass-ceramic showing a continuous dissolution of the residual amorphous phase and a preferential dissolution of the $Na_2Mg(PO_4)_3$ crystals. Combining molecular and biochemical analysis, it may be suggested that, on GC-ICEL slices, a stimulation of hMSCs differentiation over proliferation occurred. Finally, the presence of a higher expression of bone related genes in cells cultured on GC-ICEL compared to cells on TCPS, confirmed the bioactivity of this phosphate-based glass-ceramic, and might have a stimulatory effect toward osteogenesis.

Acknowledgements

The authors wish to thank Regione Piemonte (Ricerca Sanitaria Finalizzata 2006 and 2008) and the IntraEuropean Marie Curie fellowship (BIORESS) for supporting this research.

References

[1] Hench LL, Splinter RJ, Allen WC, Greenlee TK. Bonding mechanisms at the interface of ceramic prosthetic materials. J Biomed Mater Res 1971;5:117-141.

[2] Hench LL. The story of Bioglass®. J Mater Sci:Mater Med 2006;17:967-968.

[3] Gao H, Tan T, Wang D. Dissolution mechanism and release kinetics of phosphate controlled release glasses in aqueous medium. J Controll Rel 2004;96:29-36.

[4] Abou Neel EA, Mizoguchi T, Ito M, Bitar M, Salih V, Knowles JC. In vitro bioactivity and gene expression by cells cultured on titanium dioxide doped phosphate-based glasses. Biomaterials 2007;28:2967-2977.

[5] Abou Neel EA, Knowles JC. Physical and biocompatibility studies of novel titanium dioxide doped phosphate-based glasses for bone tissue engineering applications. J Mater Sci:Mater Med 2008;19:377-386.

[6] Abou Neel EA, Ahmed I, Pratten J, Nazhat SN, Knowles JC. Characterisation of antibacterial copper releasing degradable phosphate glass fibres. Biomaterials 2005;26:2247-2254.

[7] Ahmed I, Collins CA, Lewis MP, Olsen I, Knowles JC. Processing, characterisation and biocompatibility of iron-phosphate glass fibres for tissue engineering. Biomaterials 2004;25:3223-3232.

[8] Abou Neel EA, Ahmed I, Blaker JJ, Bismarck A, Boccaccini AR, Lewis MP, Nazhat SN, Knowles JC. Effect of iron on the surface, degradation and ion release properties of phosphate-based glass fibres. Acta Biomater 2005;1:553-563.

[9] Bunker BC, Arnold GW, Wilder JA. Phosphate glass dissolution in aqueous solutions. J Non-Cryst Solids 1984;64:291-316.

[10] Valappil SP, Pickup DM, Carroll DL, Hope CK, Pratten J, Newport RJ, Smith ME, Wilson M, Knowles JC. Effect of silver content on the structure and antibacterial activity of silver-doped phosphate-based glasses. Antimicrob Agents Chemother 2007;51:4453-4461.

[11] Sanzana ES, Navarro M, Macule F, Suso S, Planell JA, Ginebra MP. Of the in vivo behavior of calcium phosphate cements and glasses as bone substitutes. Acta Biomater 2008;41924-1933.

[12] Gilchrist T, Glasby MA, Healy DM, Kelly G, Lenihan DV, McDowall KL, Miller IA. In vitro nerve repair - in vivo. The reconstruction of peripheral nerves by entuhulation with biodegradeable glass tubes - a preliminary report. Br J Plast Surg 1998;51:231-237.

[13] Jeans LA, Gilchrist T, Healy D. Peripheral nerve repair by means of flexible biodegradable glass fibre wrap: a comparison with microsurgical epineuril repair. J Plast Reconstr Aesthet Surg 2007;60:1302-1308.

[14] Shah R, Sinanan ACM, Knowles JC, Hunt NP, Lewis MP. Craniofacial muscle engineering using a 3-dimensional phosphate glass fibre construct. Biomaterials 2005;26:1497-1505.

[15] Chen QZ, Rezwan K, Armitage D, Nazhat SN, Boccaccini AR. The surface functionalization of 45S5 Bioglass-based glass-ceramic scaffolds and its impact on bioactivity. J Mater Sci:Mater Med 2006;17:979-987.

[16] Yao J, Radin S, Reilly G, Leboy PS, Ducheyne P. Solution-mediated effect of bioactive glass in poly (lactic-co-glycolic acid)-bioactive glass composites on osteogenesis of marrow stromal cells. J Biomed Mater Res A 2005;75:794-801.

[17] Vitale-Brovarone C, Bretcanu O, Verné E. Synthesis and characterization of a degradable phosphate glass and its application as resorbable bone graft. Submitted to J Mater Sci:Mater Med.

[18] ISO 10993-14:2002 standard. Biological evaluation of medical devices: identification and quantification of degradation products from ceramics.

[19] Kokubo T, Takadama H. How useful is SBF in predicting in vivo bone bioactivity? Biomaterials 2006;27:2907-2915.

[20] Causa F, Netti PA, Ambrosio L, Ciapetti G, Baldini N, Pagani, S, Martini D, Giunti A. Polycaprolactone/hydroxyapatite composites for bone regeneration*: In vitro* characterization and human osteoblast response. J Biomed Mater Res 2006;76:151-162.

[21] Mouritzen P, Noerholm M, Nielsen PS. ProbeLibrary: A new method for faster design and execution of quantitative real-time PCR. Nat Methods 2005;4:313-316.

[22] Vitale Brovarone C, Verné E, Robiglio L, Appendino P, Bassi F, Martinasso G, Muzio G, Canuto RA. Development of glass-ceramic scaffolds for bone tissue engineering: characterisation, proliferation of human osteoblasts and nodule formation. Acta Biomater 2007;3:199-208.

[23] Patel A, Knowles JC. Investigation of silica-iron-phosphates glasses for tissue engineering. J Mater Sci:Mater Med 2006;17:937-944.

[24] Hench LL, Polak JM, Xynos ID, Buttery LDK. Bioactive materials to control cell cycle. Mater Res Innov 2000;3:313-323.

[25] Xynos ID, Edgar AJ, Buttery LDK, Hench LL, Polak JM. Ionic products of bioactive glass dissolution increase proliferation of human osteoblasts and induce insulin-like growth factor II mRNA expression and protein synthesis. Biochem Biophys Res Commun 2000;276:461-465.

[26] Hench LL. Genetic design of bioactive glass. J Eur Ceram Soc 2008, doi: 10.1016/j.jeurceramsoc.2008.08.002

[27] Cao W, Hench LL. Bioactive materials. Ceram Int 1996;22:493-507.

[28] Kasuga T, Sawada M, Nogami M, Abe Y. Bioactive ceramics prepared by sintering and crystallization of calcium phosphate invert glasses. Biomaterials 1999;20:1415-1420.

[29] Monem AS, ElBatal HA, Khalil EMA, Azooz MA, Hamdy YM. In vivo behavior of bioactive phosphate glass-ceramics from the system P_2O_5–Na_2O–CaO containing TiO_2, J Mater Sci:Mater Med 2008;19:1097-1108.

[30] Sun JS, Chang WHS, Chen LT, Huang YC, Juang LW, Lin FH. The influence on gene-expression profiling ofosteoblasts behaviour following treatment with the ionic products of sintered β-dicalcium pyrophosphate dissolution. Biomaterials 2004;25:607-616.

[31] Au AY, Au RY, Al-Talib TK, Eves B, Frondoza CG. Consil® bioactive glass particles enhance osteoblast proliferation and maintain extracellular matrix production in vitro. J Biomed Mater Res A 2008;86:678-684.

[32] Augst A, Marolt D, Freed LE, Vepari C, Meinel L, Farley M, Fajardo R, Patel N, Gray M, Kaplan DL, Vunjak-Novakovic G. Effects of chondrogenic and osteogenic regulatory factors on composite constructs grown using human mesenchymal stem cells, silk scaffolds and bioreactors. J R Soc Interface 2008;5:929-39.

[33] Jones JR, Tsigkou O, Coates EE, Stevens MM, Polak JM, Hench LL. Extracellular matrix formation and mineralization on a phosphate-free porous bioactive glass scaffold using primary human osteoblast (HOB) cells. Biomaterials 2007;28:1653-1663.

[34] Knabe C, Stiller M, Berger G, Reif D, Gildenhaar R, Howlett CR, Zreiqat H. The effect of bioactive glass ceramics on the expression of bone-related genes and proteins in vitro. Clin Oral Implants Res 2005;16:119-127.

[35] Knabe C, Houshmand A, Berger G, Ducheyne P, Gildenhaar R, Kranz I, Stiller M. Effect of rapidly resorbable bone substitute materials on the temporal expression of the osteoblastic phenotype in vitro. J Biomed Mater Res A 2008;84:856-868.

Tables

Table 1

List of primers and probes selected to analyse the expression of genes related to the bone cell differentiation.

Gene (Symbol) - NCBI reference number		Primer sequence (5'-3')	Probe	Detection limit (μg)
Glyceraldehyde 3-phosphate dehydrogenase (GAPDH) - NM_002046.3	Sense Antisense	agccacatcgctcagacac gcccaatacgaccaaatcc	#60	3×10^{-12}
Alkaline phosphatase (ALPL) - NM_000478.3	Sense Antisense	gggtcagctccaccacaa gcattggtgttgtacgtcttg	#52	2.1×10^{-11}
Osteocalcin (BGLAP) - NM_199173.2	Sense Antisense	ggcgctacctgtatcaatgg tcagccaactcgtcacagtc	#1	4×10^{-12}
Type 1 collagen, alpha 1 chain (COL1A1) - NM_000088.3	Sense Antisense	cccctggaaagaatggagat aatcctcgagcaccctga	#60	3.7×10^{-13}

Table 2

Weight losses of GC-ICEL samples after soaking in SBF, Tris-HCl and water.

Soaking medium	Weight losses	Soaking time			
		7 days	1 month	2 month	3 month
SBF	Λ_W (%)	4.2 ± 0.6	10.5 ± 0.6	11.0 ± 1.0	12.0 ± 1.2
	Λ_S (mg·cm^{-2})	8.0 ± 0.9	21.3 ± 1.4	22.6 ± 2.0	25.0 ± 1.1
Tris-HCl	Λ_W (%)	6.1 ± 0.2	15.9 ± 1.2	28.0 ± 0.3	30.0 ± 1.4
	Λ_S (mg·cm^{-2})	12.0 ± 0.1	30.2 ± 2.0	53.6 ± 2.0	63.1 ± 2.0
Water	Λ_W (%)	29.0 ± 2.0	47.0 ± 1.6	48.0 ± 0.3	49.0 ± 1.5
	Λ_S (mg·cm^{-2})	55.7 ± 1.8	76.5 ± 1.5	93.5 ± 2.0	97.3 ± 2.0

Figure

Fig. 1. Diffraction pattern of GC-ICEL after soaking in different aqueous media for 1 week (a) and 3 months (b).

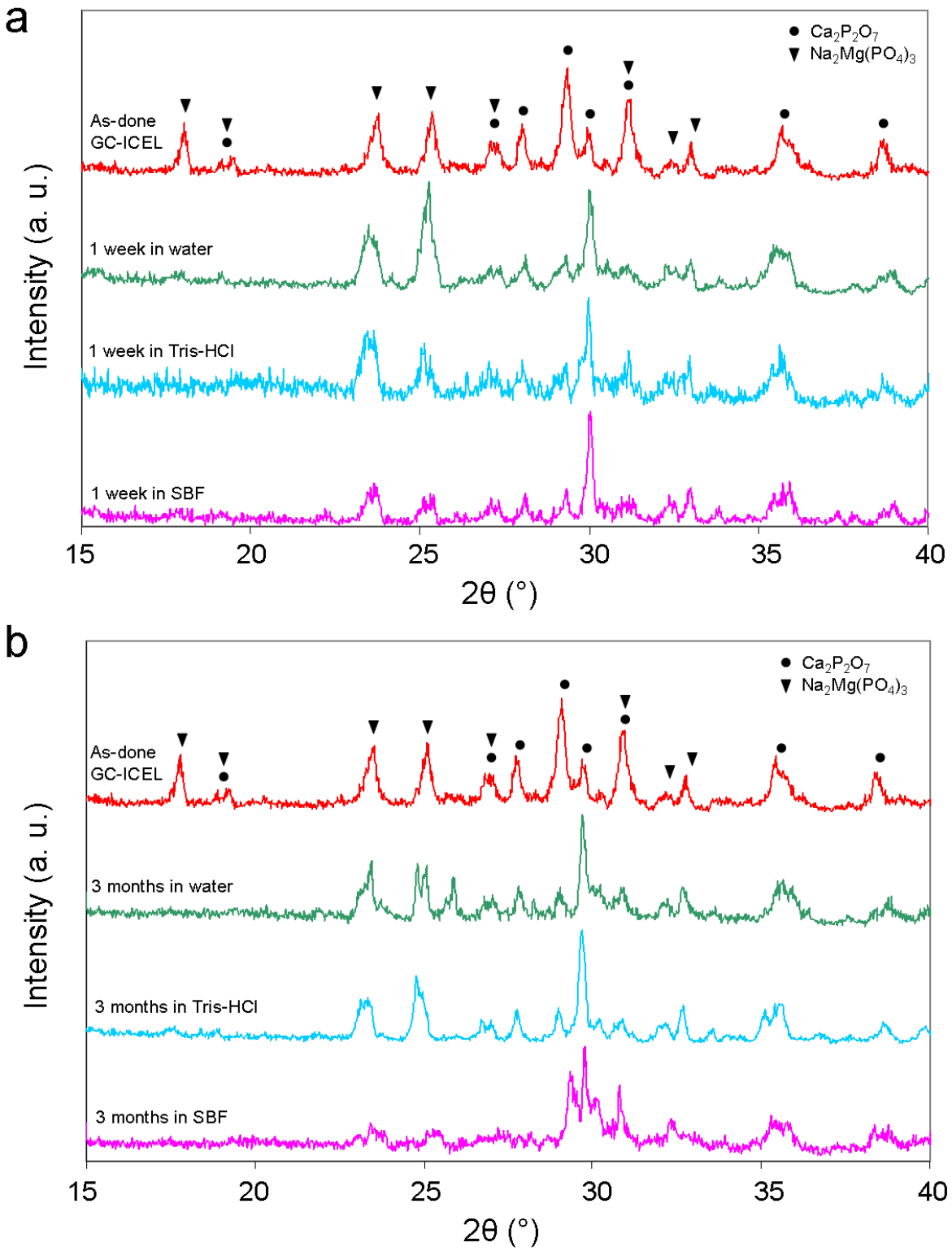

Fig. 2. Micrographs of as-done GC-ICEL at different magnifications: (a) image at 50x, (b) image at 300x.

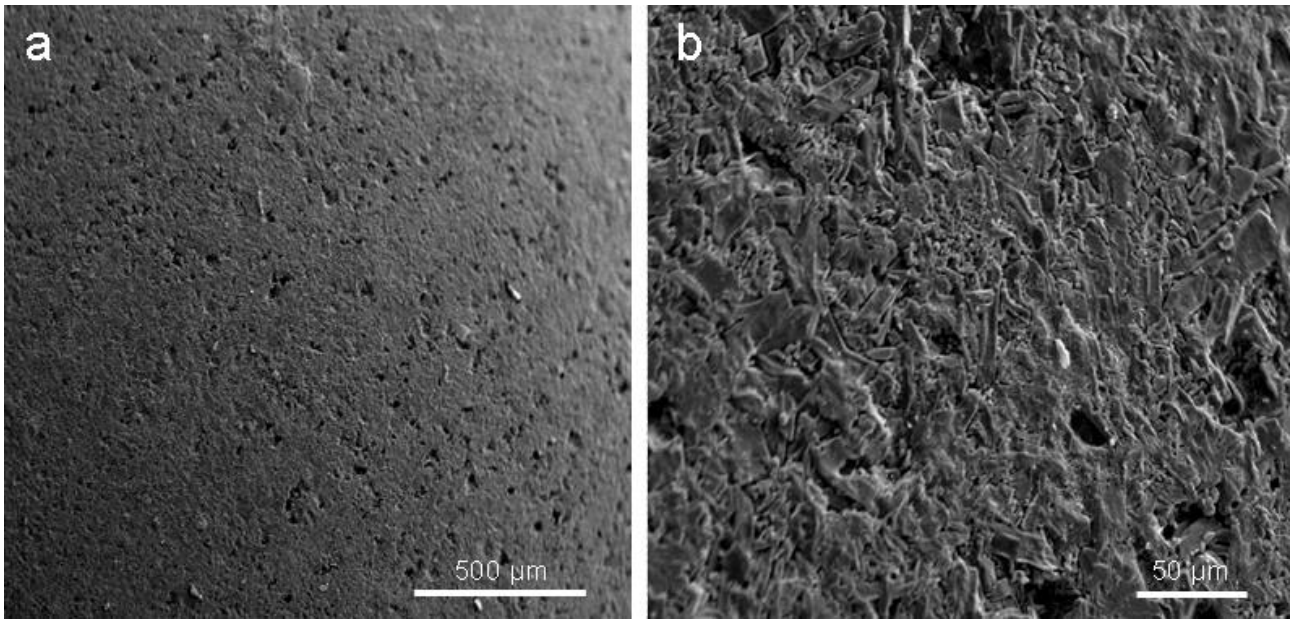

Fig. 3. GC-ICEL surface after 7 days in water (magnification: 350x).

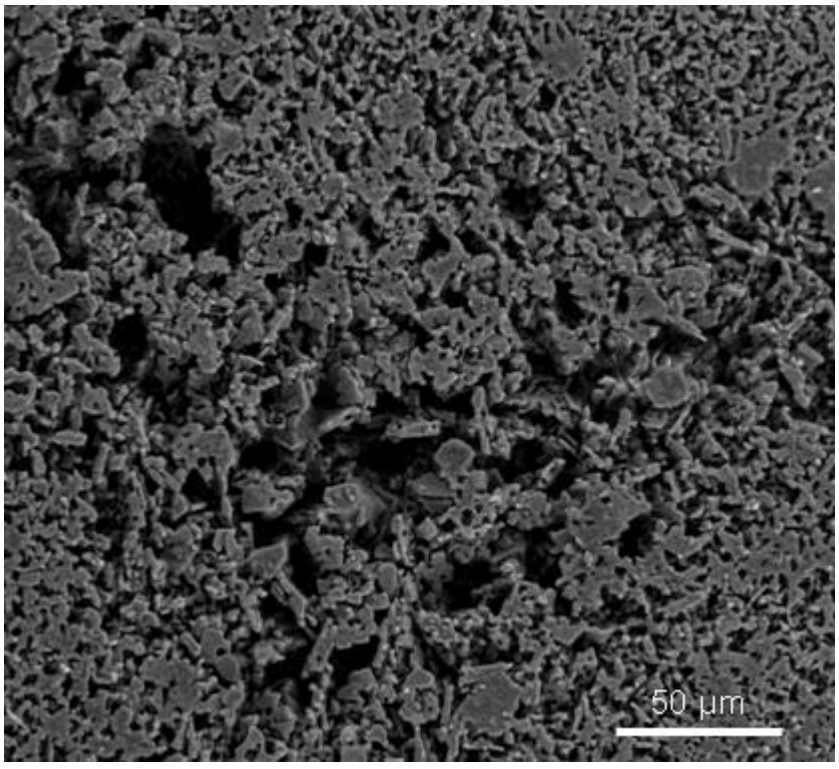

Fig. 4. GC-ICEL surface after 7 days in SBF (magnification: 10,000x).

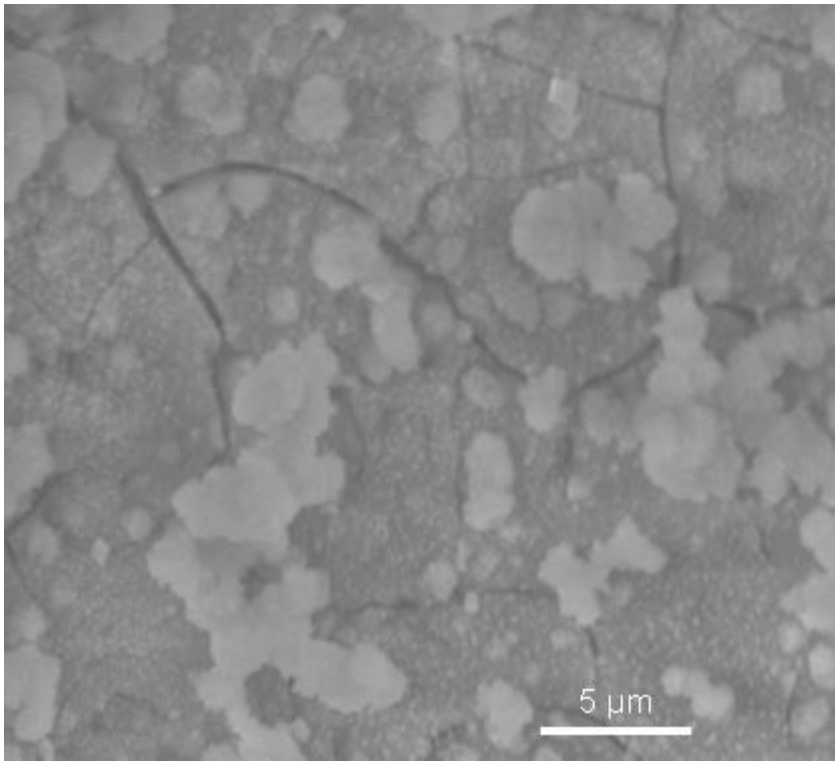

Fig. 5. Weight loss of GC-ICEL after soaking in distilled water, Tris-HCl and SBF: assessment of (a) Λ_W and (b) Λ_S.

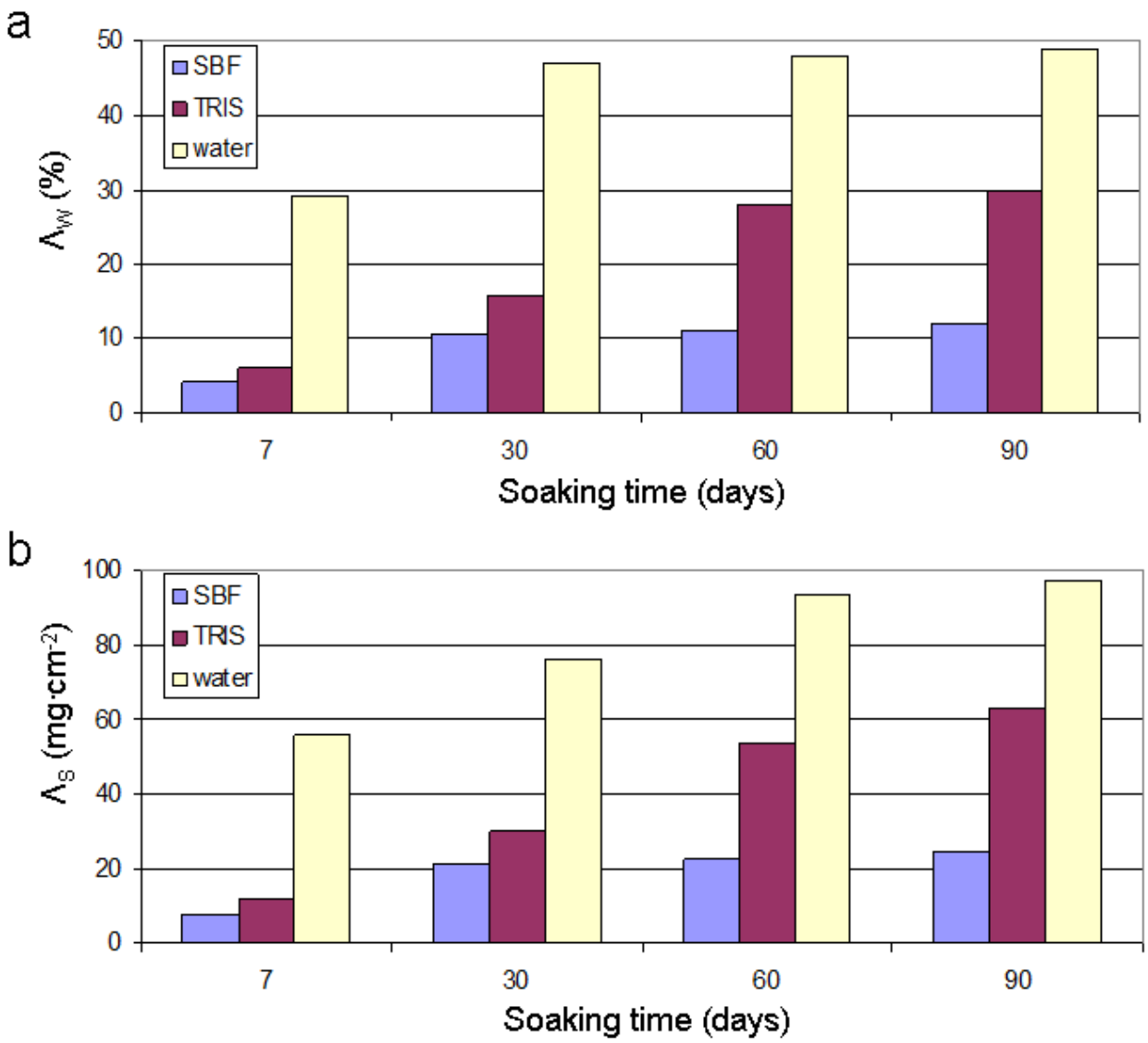

Fig. 6. Variations of medium pH during the cell culture period.

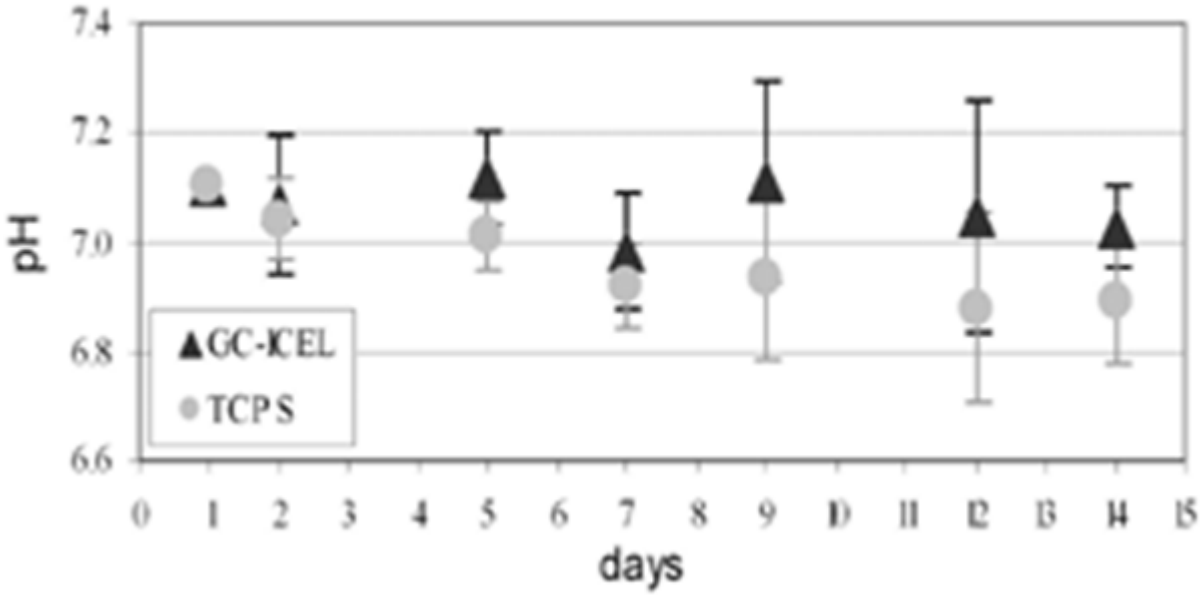

Fig. 7. Cell adhesion at 24 h from seeding: cell morphology by acridine orange (a,b) and cytoskeleton by phalloidine-TRITC (c,d) of cells grown on GC-ICEL (a,c) and TCPS (b,d).

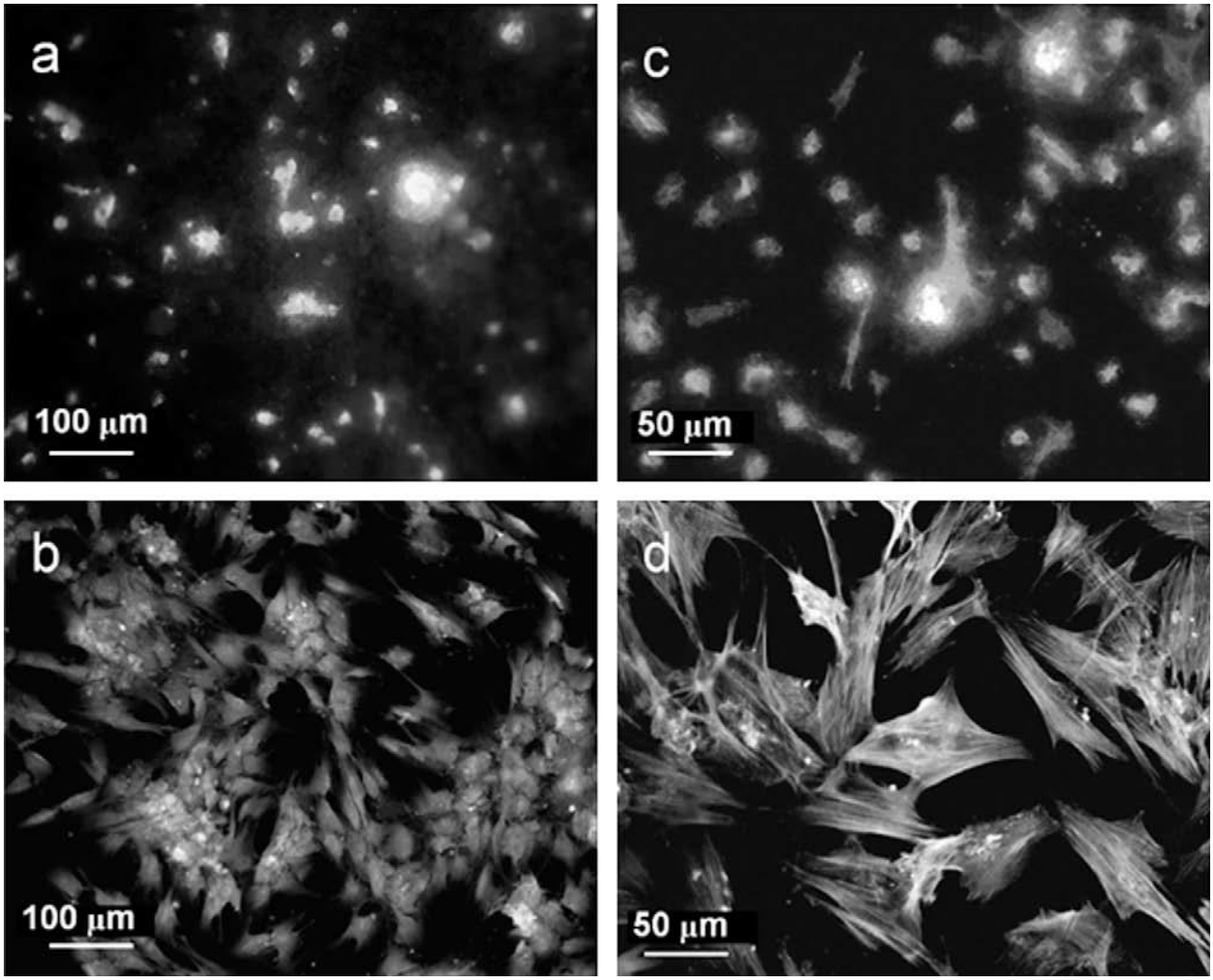

Fig. 8. Cell adhesion at 24 h from seeding: SEM images of cells on GC-ICEL surfaces.

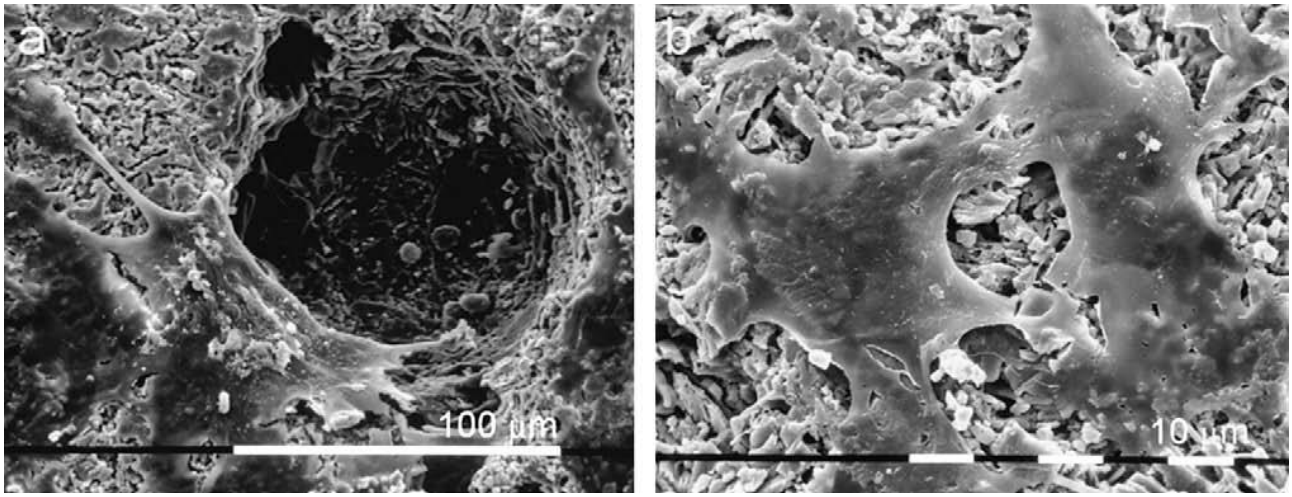

Fig. 9. Viability by Alamar test (a) and proliferation by Picogreen test (b) of hMSC on GC-ICEL substrate at different time points (RFU= Relative Fluorescence Units). * $p < 0.05$ on TCPS 1d *vs* 7d (a,b) and 7d *vs* 14d (a)

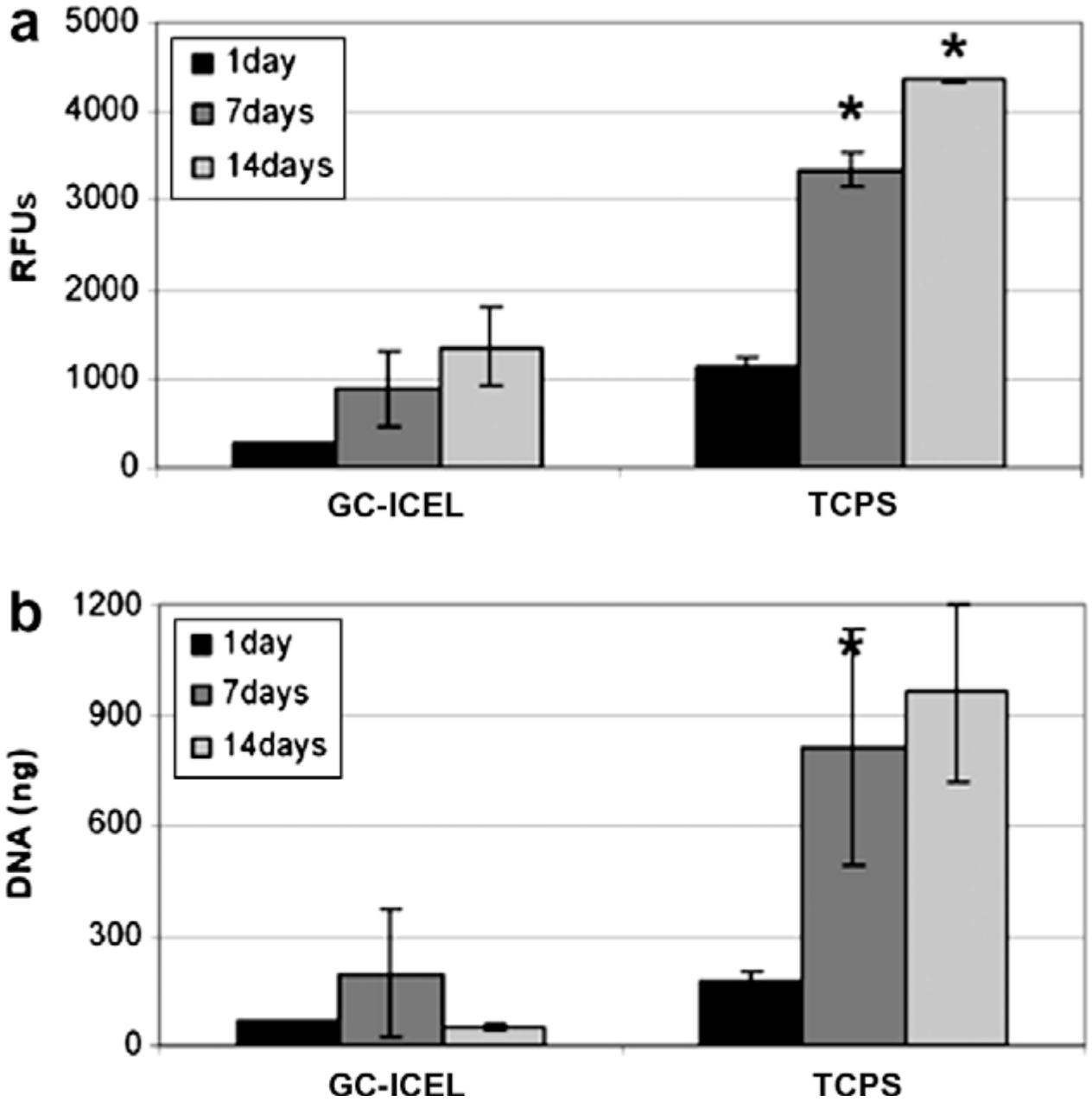

Fig. 10. SEM analysis of GC-ICEL after pre-wetting treatment (a,b), at 7 days (c,d) and at 14 days (e,f) of culture with hMSCs.

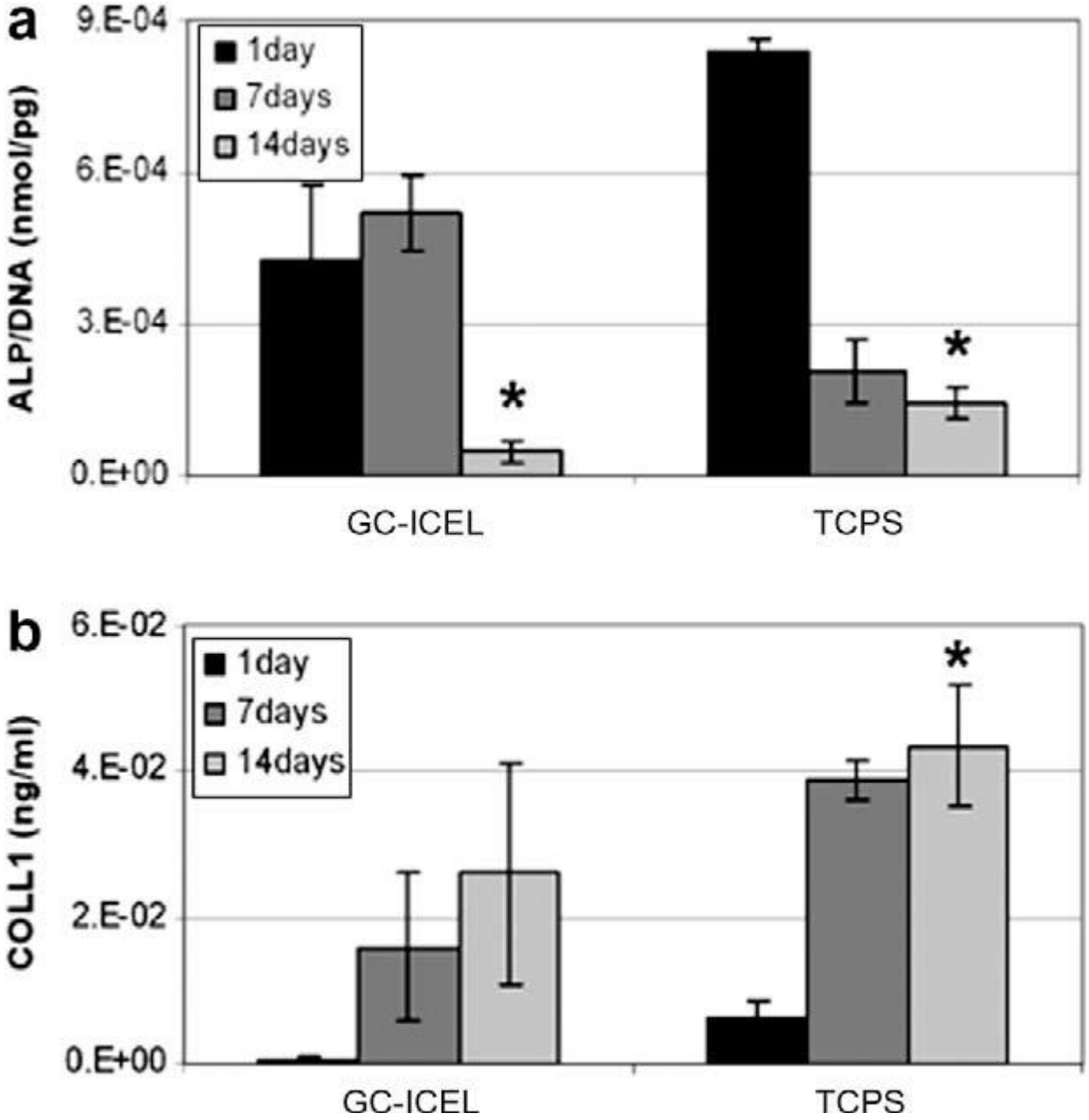

Fig. 11. Osteogenic differentiation markers: alkaline phosphatase activity from lysate (a) and collagen I release in the culture supernatant (b). * $p < 0.05$ on TCPS 1d *vs* 7d (a,b) and on GC-ICEL 7d *vs* 14d (a).

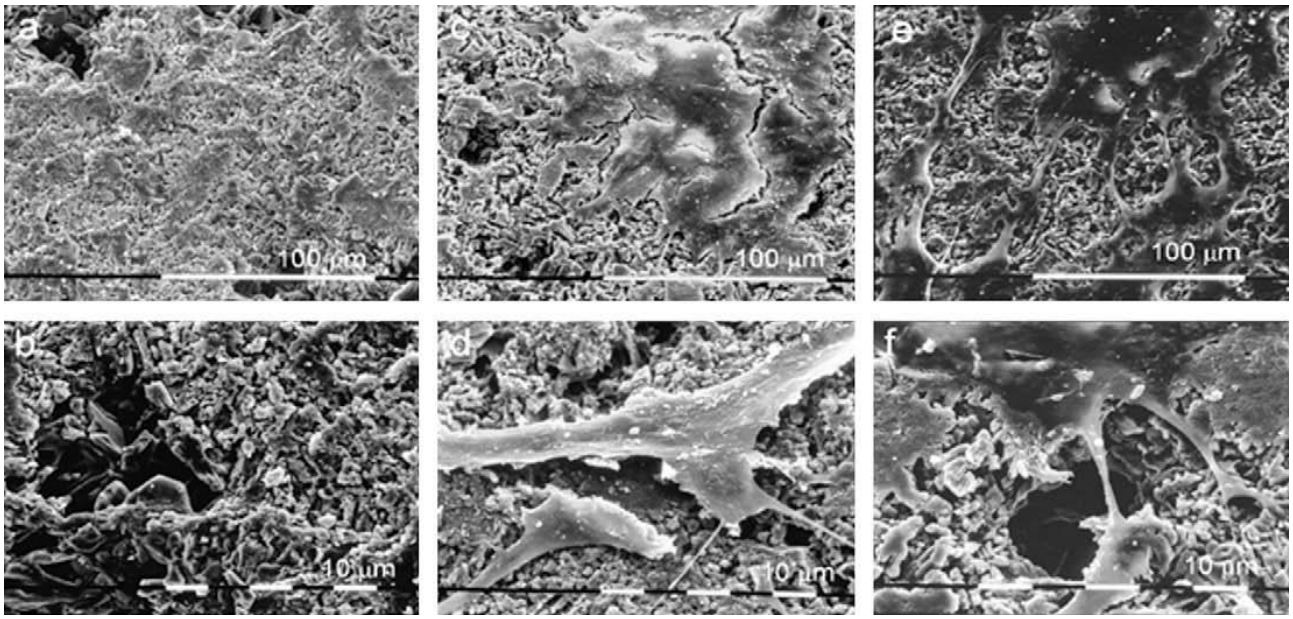

Fig. 12. Gene expression analysis of hMSCs cultured on GC-ICEL.